PORT SAID ENGINEERING RESEARCH JOURNAL

Faculty of Engineering - Port Said University

Volume (20) No. 2 September 2016 pp: 40:53

A Developed Flexibility-Based Beam Column Element for Nonlinear Analysis of Reinforced Concrete Seismic Resisting Frames

Abdel Khalik , A. K. [1]; Hassan, H. M.[2] and Sallam, E. A.[3]

ABSTRACT

A flexibility-based reinforced concrete beam column element is developed to study the nonlinear static and dynamic response of reinforced concrete seismic resisting frames. To model beam to column flexible connections and rigid zones that formed from beam to column intersections, end springs and end offsets are included in the element formulation, respectively. The element flexibility matrix is formed by integration of in-span section flexibilities using conventional force relations using the Simpson's method. Each cross section in the element span is subdivided into concrete and steel fibers/layers with the assumption of linear strain distribution over the section depth. The effects of shear and bond slip are neglected in the element formulation. The formulated beam column element is implemented into a developed finite element program. For the sake of verification, a series of correlations studies against members and structures available in the literature subjected to either monotonic or cyclic loads were investigated and showed a good accuracy. The proposed element can be used in nonlinear static and dynamic analysis of seismic resisting systems.

Keywords: RC frames, static/dynamic response, flexibility method, end springs, end offsets.

1. Introduction

The nonlinear static and dynamic analyses of structures are used extensively in the assessment of existing structures in high risk zones and in the development of appropriate retrofit strategies. Modeling of structures by Finite Element Method (FEM) is the best compromise between simplicity and accuracy. The most promising elements for the nonlinear analysis of reinforced concrete members are, presently, flexibility-based fiber elements. The first flexibility-based fiber element was proposed by Kaba [1] and Filippou [2]. It follows the outline of the flexibility approach using the force interpolation functions in the determination of element flexibility matrix. Only uniaxial bending is taken into account. In the state determination phase of nonlinear analysis, the section deformations are computed from element deformations with the flexibility–dependent deformations shape functions. The integral over the element length are evaluated by subdividing the element into equally space segments and assuming a linear flexibility distribution between segments. The model yielded a very promising results, but convergence issues and lack of theoretical clarity and contains several inconsistences that cause numerical problems.

A beam column finite element model for the analysis of reinforced concrete members under cyclic loading conditions that induce biaxial bending and axial force was proposed by Taucer [3]. The formulation of the element is based on mixed method. A special flexibility-based state determination algorithm was proposed for the computation of the stiffness matrix and resisting forces of beam column element. A reinforced concrete beam finite element that explicitly accounts for the slip between the reinforcing bars and the surrounding concrete was proposed by Monti [4]. The element formulation combines the fiber-section model with the finite-element model of a reinforcing bar with continuous slip. The steel fiber strains were computed as the sum of two contributions, the rebar deformation and anchorage slip. The model was applied to different cross-section shapes under biaxial bending and both monotonic and cyclic loads. Strategies for equilibrium-based formulations along with a solution scheme based on the secant stiffness matrix and method of direct iteration , techniques to overcome the difficulty of softening in nonlinear analysis of reinforced concrete members, mesh objectivity and a simplified model for shear distribution over the height of a cracked section were investigated by Valipour [5].

A fiber beam column element able to reproduce the non-linear behavior of squat structures was formulated by Diotallevi [6]. Its main characteristics are substantially the flexibility formulation and the constitutive relationship characterized by a rotating smeared crack model. The model was able to reproduce flexure and shear non-linear response and above all, the coupling between flexure and shear in the non-linear range [6]. A planar frame fiber element

[1] *Professor of Concrete Structures, Civil Engineering Department, Faculty of Engineering, Suez Canal University, Ismailia, Egypt*

[2] *Professor of Concrete Structures, Civil Engineering Department, Faculty of Engineering, Port Said University, Port Said, Egypt*

[3] *PhD student, Civil Engineering Department, Faculty of Engineering, Port Said University, Port Said, Egypt*

Email: Ezat_sallam@yahoo.com

model including a fully coupled shear–bending–axial forces sectional response and a flexibility-based formulation for curved elements was proposed by Mohr [7]. The A flexibility-based frame element includes shear deformability, which is connected with the cross-section model. The model has shown to fit the experimental results with more accuracy than non-linear solutions based on Navier-Bernouilli and Timoshenko theories and other formulations, which provide stiffer behavior than that experimentally observed in shear dominated specimens [7].

A beam column model for seismic analysis of reinforced concrete frames was presented by El-Heweity [8]. The model is a simplified version of the flexibility-based fiber models. In his model, only the two end sections are subdivided into fibers and uniaxial material models that consider the various behavioral characteristics of steel and concrete under cyclic loading conditions were assigned for the cross section fibers. The inelastic lengths at the ends of the model were divided into two inelastic zones; cracking and yielding. The inelastic lengths vary according to the loading history and were calculated in every load increment. The overall response of the RC member is estimated using preset flexibility distribution functions along the element length [8].

From the available literature, modeling of framed systems requires improved finite elements reducing number of elements and containing different modeling capabilities. In the present study, an improved formulation and state determination for general purpose flexibility-based reinforced concrete beam column element with end springs and/or end offsets were presented.

2. Finite Element Formulation

Based on the small deformation assumption, Navier-Bernoulli theory is adopted for distribution of axial strain over the section where the effects of shear on yielding and fracture of axial fibers are neglected. Perfect bond is assumed between reinforcing bar and surrounding concrete. The procedure presented by Taucer [3] is used the present formulation. A cantilever clamped end configuration is used in the element formulation due its simplicity and it will produce full flexibility coefficients for one beam ends, Figure 1a.

2.1 Element Level

Three sets of equations resulting from the application of equilibrium, compatibility and constitutive laws are established based on the Newton solution schemes and are consistent with the tangent stiffness approach. Figure 1c shows a 2-node frame element with three degrees of freedom at each node (two translations and one rotation) subjected to the distributed loads w (x). Considering an arbitrary section located at x along the element, equilibrium for configuration i-s (Figure 2) gives [3]:

$$D(x) = b(x)\, Q_1 + FD(x) \quad (1)$$

where, D(x) is the generalized section forces; b(x) is the force interpolation matrix; Q1 is a vector of end forces for member end (1); and FD(x) is the vector of sectional forces from in-span loading.

$$D(x) = [N(x) \quad M(x)]^T \quad (2)$$

$$b(x) = \begin{bmatrix} -1 & 0 & 0 \\ 0 & x & -1 \end{bmatrix} \quad (3)$$

$$Q_1 = [Fx_1 \quad Fy_1 \quad Mz_1]^T \quad (4)$$

$$FD(x) = [0 \quad w.x^2/2]^T \quad (5)$$

For the case of two in-span loading components, as shown in Figure 2b, the vector of sectional forces from the in-span loading will be:

$$FD(x) = \left[-w_x.x \quad w_y.x^2/2\right]^T \quad (6)$$

If the term FD(x) from right side of Eq. (1) is removed, it will not violate the generality of the formulation and, hence,

$$D(x) = b(x)\, Q_1 \quad (7)$$

The incremental form of Eq. (7) is

$$\Delta D(x) = b(x)\, \Delta Q_1 \quad (8)$$

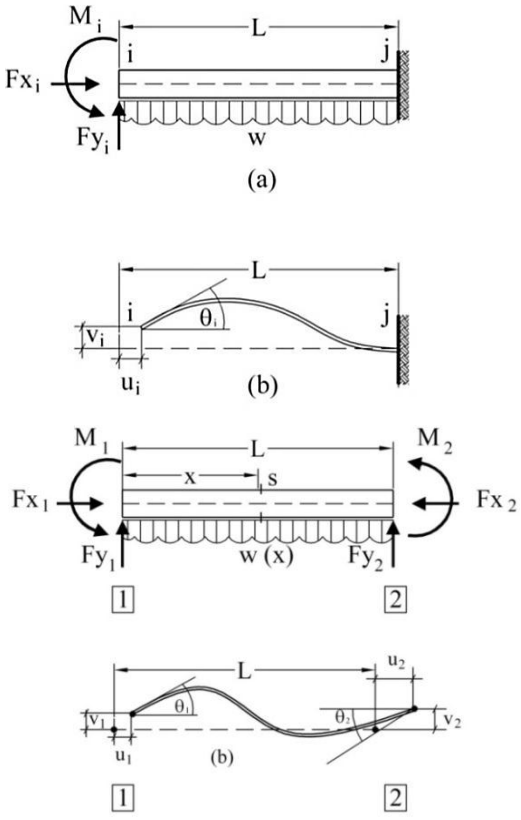

Figure 1: Cantilever clamped-end beam approach for flexibility formulation, (a) end forces and in-span loading (b) left end displacements and rotations, (c) end forces and end displacements.

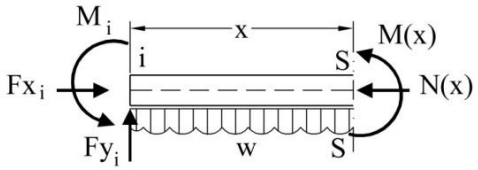

(a)

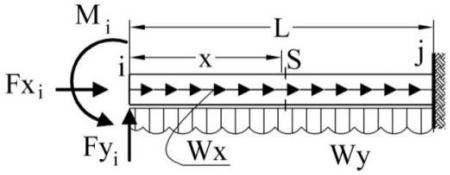

(b)

Figure 2: Element loading (a) Segment free body diagram (i-s), (b) In-span loading.

2.2 Section Level

The element is subdivided into group of equally spaced segments forming in-span sections. Each section is divided into layers for the case of plane analysis of structures, Figure 3. If Δσ represents the stress increment at a transverse layer, then equilibrium of internal stresses and tractions gives

$$\int_{\Omega} \Delta\sigma \, dA - \Delta N(x) = 0 \tag{9}$$

$$\int_{\Omega} \mathrm{y}\, \Delta\sigma \, dA + \Delta M_z(x) = 0 \tag{10}$$

where, y is the ordinate of the layer from the section elastic center of gravity. Note that, in the nonlinear analysis, the center of gravity is changed continuously accordingly with updating of layer modulus of elasticity.

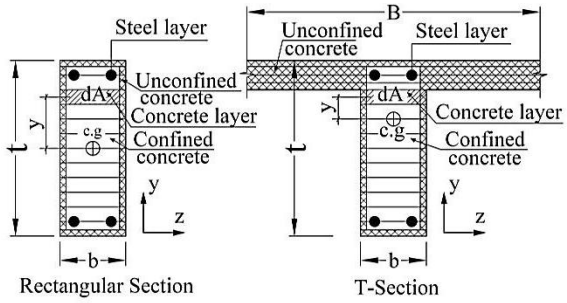

Figure 3: Discretization of concrete sections into layers/fibers.

2.3 Compatibility Equations

For the case of perfect bond using Navier-Bernoulli hypothesis, the compatibility requirement of layer strain is obtained as

$$\varepsilon(x) = \varepsilon_a(x) - y\,\phi_z(x) \tag{11}$$

where, $\varepsilon(x)$ the axial strain of fiber integration point, $\varepsilon_a(x)$ is the normal force strain, and $\phi_z(x)$ is the section curvature. The incremental strain $\Delta\varepsilon(x)$ of the fiber integration point can be found from,

$$\Delta\varepsilon(x) = \Delta\varepsilon_a(x) - y\,\Delta\phi_z(x) \tag{12}$$

If the axial stress increment $\Delta\sigma(x)$ is assumed to be a function solely of the axial strain increment $\Delta\varepsilon(x)$, then

$$\Delta\sigma(x) = E_t\,\Delta\varepsilon(x) \tag{13}$$

where, E_t is the material tangent modulus of elasticity. Regarding the material type (i.e. concrete or reinforcing steel); different fibers or layers (integration points) can have different values for E_t.

The value of $\Delta\sigma(x)$ is obtained through Eqs. (12) and (13) and substituting the results into Eqs. (9) to (10) gives:

$$\Delta N(x) = \int_{\Omega} E_t\,.\,(\Delta\varepsilon_a(x) - y\,\Delta\phi_z(x)).\,dA \tag{14}$$

$$\Delta M_z(x) = -\int_{\Omega} E_t\,.\,y.\,(\Delta\varepsilon_a(x) - y\,\Delta\phi_z(x)).\,dA \tag{15}$$

The Eqs. 14 and 15 can be expressed in the form

$$\Delta D(x) = k_s\,(x).\,\Delta d(x) \tag{16}$$

$$k_s\,(x) = \begin{bmatrix} \int_{\Omega} E_t\,dA & -\int_{\Omega} y.E_t\,dA \\ -\int_{\Omega} y.E_t\,dA & \int_{\Omega} y^2.E_t\,dA \end{bmatrix} \tag{17}$$

where, $k_s\,(x)$ is the section stiffness matrix and $\Delta d(x)$ is the vector of section incremental strains $\{\Delta\varepsilon_a(x) \quad \Delta\phi_z(x)\}^T$. The flexibility matrix of the section which relates the section strains $\Delta d(x)$ with section forces $\Delta D(x)$ is obtained by inverting the section stiffness matrix, that is

$$\Delta d(x) = f_s\,\,(x).\,\Delta D(x) \tag{18}$$

$$f_s^t(x) = \left[k_s\,(x)\right]^{-1} \tag{19}$$

Using the principle of virtual work for a cantilever configuration clamped at end 2 and subjected to a virtual load vector ΔQ_1 at end 1 (Figure 1-b) gives

$$\Delta q_1 = \int_0^l \mathrm{b}^T(\mathrm{x}).\,\Delta d(x)\mathrm{dx} \tag{20}$$

If Eqs. 3.8 and 3.18 are substituted in Eq. 3.20, then

$$\Delta q_1 = \left(\int_0^l \mathrm{b}^T(\mathrm{x}).\,f_s\,\,(x).\,b(x)\,\,\mathrm{dx}\right)\Delta Q_1 \tag{21}$$

$$\text{Or} \quad \Delta q_1 = F_{11}\,\Delta Q_1 \tag{22}$$

where, Δq_1 is the generalized displacement increment at end "1", Then the tangent flexibility sub-matrix at end "1" for the beam column element can be found from,

$$F_{11} = \int_0^l \mathrm{b}^T(\mathrm{x}).\,f_s\,\,(x).\,b(x)\,\,\mathrm{dx} \tag{23}$$

After the tangent flexibility sub-matrix F_{11} at end "1" formulated, then the stiffness matrix of the beam column element can be found from,

$$[K_e] = \begin{bmatrix} [F_{11}]^{-1} & [F_{11}]^{-1}.\Gamma \\ \Gamma^T.[F_{11}]^{-1} & \Gamma^T.[F_{11}]^{-1}.\Gamma \end{bmatrix} \tag{24}$$

where, $F_{11}$is (3x3) matrix, and Γ is a transformation (2x3) matrix takes the form

$$\Gamma = \begin{bmatrix} -1 & 0 & 0 \\ 0 & L & -1 \end{bmatrix} \quad (25)$$

2.4 Flexibility-Based Beam Column Element with End Springs

Typically, in modeling the response of reinforced-concrete structures to earthquake loading, it is assumed that beam column joints remain rigid and elastic. However, laboratory testing of building subassemblage with design details typical of pre-1970's construction shows that joints with little to no transverse reinforcement and relatively high shear and bond-stress demand exhibit severe stiffness and strength loss [9]. A flexibility-based beam column element with additional end springs shown in Figure 4. Referring to element formulation presented in subsection 2.1 to 2.3, the member end "1" vector of generalized displacement Δq_1 is divided into two components; one due to beam column element stiffness for the beam column element between the two end springs $\Delta {q_1}^{BC}$, and the other due to rigid body translations and rotations $\Delta {q_1}^{RB}$ from the attached end springs. Then, end "1" generalized displacements could be calculated form Eqs. 26 to 29 as follows

$$\Delta q_1 = \Delta {q_1}^{BC} + \Delta {q_1}^{RB} \quad (26)$$

$$\Delta {q_1}^{BC} = \int_0^l \mathrm{b}^T(\mathrm{x}).\Delta d(x)\,\mathrm{dx} \quad (27)$$

$$\Delta q_1 = \left[{F_{11}}^{BC} + {F_{11}}^{RB}\right]\Delta Q_1 \quad (28)$$

$$\mathrm{F_{11}}^{BC} = \int_0^l \mathrm{b}^T(\mathrm{x}).\Delta d(x)\,\mathrm{dx} \quad (29)$$

$$\mathrm{F_{11}}^{RB} = \begin{bmatrix} 0 & 0 & 0 \\ 0 & \left(\frac{L^2}{k_{s2}}\right) & \left(\frac{-L}{k_{s2}}\right) \\ 0 & \left(\frac{-L}{k_{s2}}\right) & \left(\frac{1}{k_{s1}}+\frac{1}{k_{s2}}\right) \end{bmatrix} \quad (30)$$

where, k_{s1} and k_{s2} are the tangent rotational stiffnesses for left and right end springs, respectively.

2.5 Flexibility-Based Beam Column Element with End Offsets

The structural length is measured from the center lines of connected elements. The effect of rigid zone at the intersection of columns and beams is considered as rigid offsets and will reduce the effective structural span (Figure 5). In order to take the effect of end offsets in the formulation, the stiffness matrix $[K_e]$ for the beam column element is modified by means of multipoint constraint matrix [A]. Consider that a_1 and a_2 are the end offsets for end (1) and (2) respectively, the matrix [A] which includes the effect of end offsets is [6x6] matrix. The diagonal terms are set to unity while all the remaining elements are set to 0 except the following elements:

$$A(2,3) = a_1 \quad and \quad A(5,6) = -a_2 \quad (31)$$

Then the modified element stiffness matrix is calculated from:

$$\overline{[K_e]} = [A]^T[K_e][A] \quad (32)$$

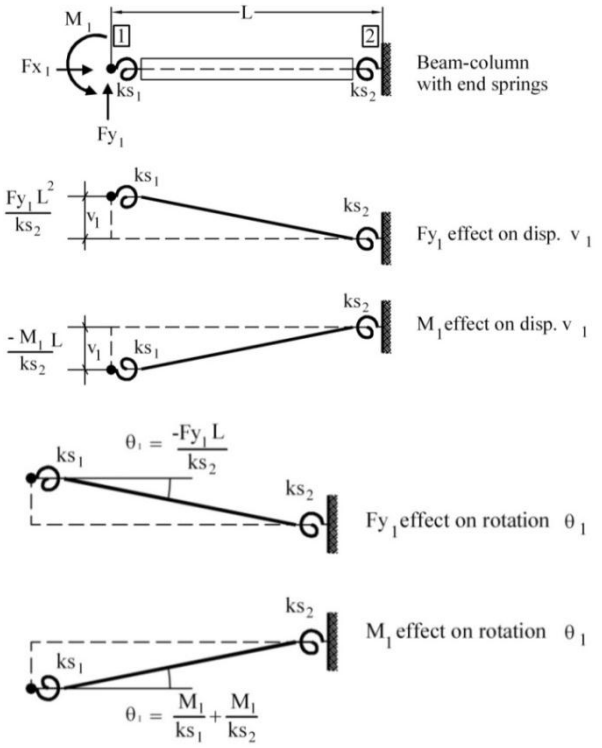

Figure 4: Rigid body deformations of beam-column element with end rotational springs.

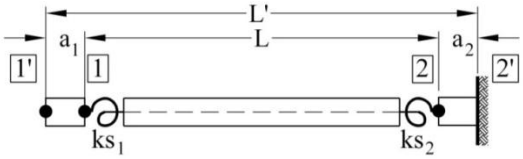

Figure 5: Beam column with end springs and end offsets.

3. Element Resistance Determination

The determination of beam column resistance forces using flexibility approach undergoes two major steps. The first: section state determination, in which each section forming the beam column element is evaluated to determine its resistance according to the current applied sectional forces, accordingly, the section residual forces are then determined. Then, the section residual strains are evaluated. The second: element state determination, in which and using section residual strains, the element residual end displacements are calculated by means of integration the section residual strains along element length. Thereafter, element

residual end forces are calculated. Finally, the element resisting forces are calculated by subtracting the current element residual forces from applied element forces. This process is repeated until convergence is achieved. Consider that subscript 'i' denotes to the load step increment, and j denotes to the Newton-Raphson correction loop, then:

1. Given the current incremental nodal displacements in element local coordinates $\{\Delta u\}_j^i$, find the current element applied incremental end forces $\{\Delta Q_e\}_j^i$ from:

$$\{\Delta Q_e\}_j^i = [k_e]_j^i \{\Delta u\}_j^i \quad (33)$$

where $[k_e]_j^i$ is the element tangent stiffness matrix from the current load step.

2. If j=1, then add current incremental fixed end forces from in-span loading $\{\Delta fE\}_j^i$ to $\{\Delta Q_e\}_j^i$, then

$$\{\Delta Q_e\}_j^i = \{\Delta Q_e\}_j^i + \{\Delta fE\}_j^i \quad (34)$$

3. For each section 'k' along element length, calculate the following:
   - Calculate section forces increment $\{\Delta D(x)\}_j^i$ using:

$$\{\Delta D(x)_k\}_j^i = [b(x)]\{\Delta Q_e\}_j^i + \{UD(x)_k\}_{j-1}^i + \{\Delta FD_k\}_j^i \quad (35)$$

   where $\{UD(x)_k\}_{j-1}^i$ is the unbalanced sectional forces from the previous iteration and $\{UD(x)_k\}_0^i$=0 for the first iteration, $\{\Delta FD_k\}_j^i$ is section forces from in-span distributed load and is calculated from $=\{-w_x.x \quad w_y.x^2\}_{j=1}^i$ for the first iteration only while in the rest of iterations $\{\Delta FD_k\}_{j>1}^i = \{0 \quad 0\}_{j>1}^i$, and $[b(x)]$ is the force interpolation function.
   - With the previous section flexibility matrix$[f(x)_k]_{j-1}^i$, calculate section incremental strains $\{\Delta d(x)_k\}_j^i$ from:

$$\{\Delta d(x)_k\}_j^i = [f(x)_k]_{j-1}^i \{\Delta D(x)_k\}_j^i \quad (36)$$

   - Update current section strains $\{d(x)_k\}_j^i = \{d(x)_k\}_{j-1}^i + \{\Delta d(x)_k\}_j^i$, using the current section strains$\{d(x)_k\}_j^i = \{\varepsilon_a \quad \emptyset_z\}_j^i$, calculate current tangent section flexibility$[f(x)_k]_j^i$ corresponding to the layer tangent modulus.
   - Update concrete and steel layers strains using the current section strains from:

$$\varepsilon = \varepsilon_a - \emptyset_z y \quad (37)$$

   - Calculate the current stresses in each layer then calculate sectional resistance forces $\{DR(x)_k\}_j^i$ from:

$$\{DR(x)_k\}_j^i = \{N(x)_k = \sum_{m=1}^{nl} \sigma_m dA \qquad M_z(x)_k = \sum_{m=1}^{nl} -y.\sigma_m dA\}_j^i \quad (38)$$

   Where *nl* is number of layers.
   - Calculate residual section strain vector $\{\delta(x)_k\}_j^i$ from:

$$\{\delta(x)_k\}_j^i = [f(x)_k]_j^i\left(\{D(x)_k\}_j^i + \{\Delta D(x)_k\}_j^i - \{DR(x)_k\}_j^i\right) \quad (39)$$

   For the first iteration of each load step $\{D(x)_k\}_{j=1}^i$= previous section forces while in the rest of iterations $\{D(x)_k\}_{j>1}^i = \{DR(x)_k\}_j^i$.
4. Using section residual strains $\{\delta(x)_k\}_j^i$, calculate element residual displacements by integration of sectional residual strains:

$$\{r(x)\}_j^i = \int_0^l b(x)^T \{\delta(x)_k\}_j^i \, dx \quad (40)$$

   Simpson's rule is employed for performing the previous integral.
5. The element incremental resisting nodal forces is then calculated from:

$$\{Q_e\}_j^i = \{Q_e\}_{j-1}^i + \{\Delta Q_e\}_j^i - [k_e]_j^i \{r(x)\}_j^i \quad (41)$$

where $[k_e]_j^i$ is the updated element tangent stiffness matrix based on the updated sections flexibilities $[f(x)]_j^i$, as described in Chapter (3). For the first iteration $\{Q_e\}_0^i = 0$.

6. For each section "k" , update the unbalanced sectional forces from:

$$\{UD(x)_k\}_j^i = [b(x)]\{Q_e\}_j^i + \{\Delta FD_k\}_{j=1}^i - \{D(x)_k\}_j^i + \{D(x)_k\}_{j=1}^i \quad (42)$$

7. Finally, the element total resisting nodal force vector in local coordinates $\{f_e\}_j^i$, which will be transformed to global coordinates and used to form the resisting nodal vector $\{F\}^i$, is calculated from:

$$\{f_e\}_j^i = \{f_e\}^{i-1} + \{Q_e\}_j^i - \sum_{k=1}^{i} \{\Delta FE\}^i \quad (43)$$

   where $\sum_{k=1}^{i}\{\Delta FE\}^i$ is the total fixed end vector till the current load step. Figure 6 shows a process flowchart describing the previous procedure.

3.1 Section Centroid Update

The participation of each layer in the section stiffness $[k(x)]$ is evaluated according Eq. 17 with particular reference to the elastic centroid. The elastic centroid, Figure 7, is changed during nonlinear analysis. Fixing this elastic centroid will cause element to have non compatible axial deformations with the applied axial forces, i.e. the element will have some elongation or contraction while it is not subjected to axial forces. To reduce this formulation error, a solution technique is proposed, in which two section flexibility matrices are calculated. The first: the flexibility is calculated based on a fixed location at the section elastic centroid. This section flexibility matrix is used for all steps presented earlier through steps 2 to 7 in subsection 3. The second: flexibility matrix based on a continuous

updating of section centroid according to the current layers tangent modulus. The later flexibility is used for calculating element stiffness matrix (Eq. 19) and for steps 1 and 5 in element state determination, see subsection 3.

3.2 Element Resistance with End Springs

For beam column element having two rotational springs attached at its ends, Figure 8, the state determination described in subsections 3 is modified to account the effect of rotational springs. The process is performed by updating element end forces described by Eq. (41) using the following procedure:

1. With the element incremental forces $\{\Delta Q_e\}_j^i = \{\Delta f_{x1} \quad \Delta f_{y1} \quad \Delta M_{z1} \quad \Delta f_{x2} \quad \Delta f_{y2} \quad \Delta M_{z2}\}_j^{iT}$ which is calculated using Eq. (33), evaluate the current incremental spring rotations from:

$$\{\Delta\theta_s\}_j^i = \begin{Bmatrix} \Delta\theta_{s1} \\ \Delta\theta_{s2} \end{Bmatrix} = \begin{Bmatrix} \Delta M_{z1}/k_{s1} \\ \Delta M_{z2}/k_{s2} \end{Bmatrix} \tag{44}$$

2. Update springs rotations $\{\theta_s\}_j^i = \{\theta_s\}_{j-1}^i + \{\Delta\theta_s\}_j^i$ and calculate the current tangent spring stiffnesses ks1 and ks2. Then determine the current spring resisting moments MzR1 and MzR2.
3. Evaluate the out of balance bending moments from end springs using the following equation:

$$\begin{aligned} M_1 &= M_{1j}^{i-1} + M_{1j-1}^{i} + \Delta M_{z1} \\ M_2 &= M_{2j}^{i-1} + M_{2j-1}^{i} + \Delta M_{z2} - M_{zR2} \\ uM_1 &= (M_1 - M_{zR1}) + 0.5(M_2 - M_{zR2}) \\ uM_2 &= (M_2 - M_{zR2}) + 0.5(M_1 - M_{zR1}) \end{aligned} \tag{45}$$

where M_{1j}^{i-1} and M_{2j}^{i-1} are the beam column moments for ends 1 and 2 from the previous load step, respectively, M_{1j-1}^{i} and M_{2j-1}^{i} are the beam column resisting moments for ends 1 and 2 from previous iteration and they are the third and sixth elements of vector $\{Q_e\}_j^i$ calculated from Eq. (41), respectively. ΔM_{z1} and ΔM_{z2} are the current incremental end moments and they are the third and sixth elements of vector $\{\Delta Q_e\}_j^i$, respectively.

4. Calculate the equivalent out of balance vector resulting from end rotational springs out of balance moments:

$$\begin{aligned} R1 &= 1.5\frac{M_1 - M_{zR1}}{L} + 1.5\frac{M_2 - M_{zR2}}{L} \\ \{V_{sp}\}_j^i &= \{0 \quad R1 \quad uM_1 \quad 0 \quad -R1 \quad uM_2\}^T \end{aligned} \tag{46}$$

5. Equation (41) will be replaced with the following

$$\{Q_e\}_j^i = \{Q_e\}_{j-1}^i + \{\Delta Q_e\}_j^i - [k_e]_j^i\{r(x)\}_j^i - \{V_{sp}\}_j^i \tag{47}$$

where $[k_e]_j^i$ is the element tangent stiffness matrix without the effect of end springs, i.e. $[k_e]_j^i\{r(x)\}_j^i$ is the residual end forces from unbalanced strains along beam column sections, while $\{V_{sp}\}_j^i$ is the residual end forces from unbalanced end springs moments.

6. Then the same procedure stated in subsection 3 is adopted.

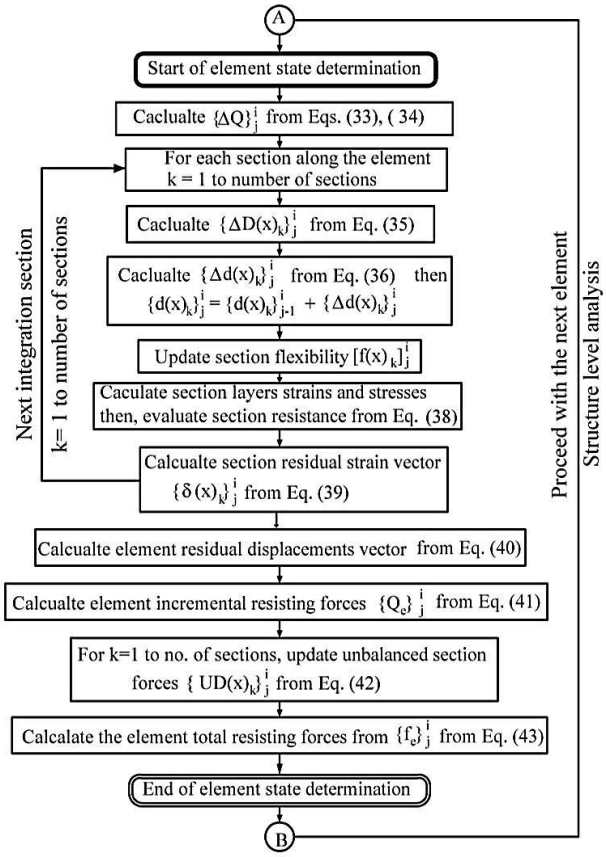

Figure 6: Reinforced Beam Column state determination procedure.

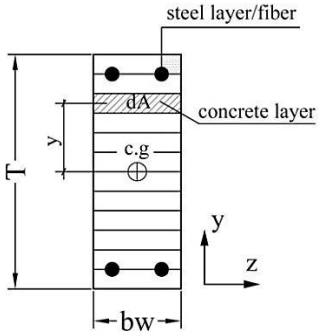

Figure 7: Division of section into layers

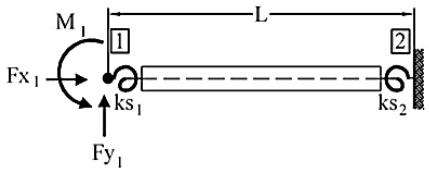

Figure 8: Reinforced concrete beam column element with end rotational springs.

3.3 State Determination with End Offsets

The state determination described earlier is modified to account the effect of rigid end offsets. The process is made by updating element end forces described by Eq. (41) by:

1. The third and sixth elements of the incremental end forces vector $\{\Delta Q_e\}_j^i$ are updated as follows:

$$\Delta Q_e(3) = -a_1.\Delta Q_e(2) + \Delta Q_e(3)_{old}$$
$$\Delta Q_e(6) = a_2.\Delta Q_e(5) + \Delta Q_e(6)_{old} \quad (48)$$

2. Finally, third and sixth elements of the resisting end force vector $\{f_e\}_j^i$ calculated using Eq. (43) is updated as follows:

$$f_e(3) = a_1.f_e(2) + f_e(3)_{old}$$
$$f_e(6) = -a_2.f_e(5) + f_e(6)_{old} \quad (49)$$

4. Material Modeling

The proposed beam column element is implemented into a developed finite element computer program **NSDA-FS** (**N**onlinear **S**tatic and **D**ynamic **A**nalysis of reinforced concrete **F**rames and **S**hear walls). The program is designed and developed in order to analyze seismic resisting systems composed from frames or coupled of frames and shear walls. Although the program is designed for 2D systems, it is also designed for the analysis of 3D systems by means of pseudo-3D technique. Different types of uniaxial stress strain curves are available in the finite element program NSDA-FS for both concrete and reinforcing steel.

4.1 Concrete Constitutive Laws

4.1.1 Compression

The stress strain curve for concrete in compression by Kent [10] for unconfined and confined concrete is used in the present study. The model generalized Hognestad [11] equation to more completely describe the post-peak stress-strain behavior. For unconfined concrete the envelope is defined by:

$$f_{ci} = f_c'\left\{2\left(\frac{\varepsilon_{ci}}{\varepsilon_{co}}\right) - \left(\frac{\varepsilon_{ci}}{\varepsilon_{co}}\right)^2\right\}, \quad \varepsilon_{ci} \le 0.002 \quad (50)$$

$$f_{ci} = f_c'\,[1 - z(\varepsilon_{ci} - \varepsilon_{co})] \quad \varepsilon_{ci} > 0.002 \quad (51)$$

$$z = \frac{0.5}{\varepsilon_{50u} - \varepsilon_{co}} \quad (52)$$

$$\varepsilon_{50u} = \frac{3 + 0.29f_c'}{145f_c' - 1000} \quad , f_c' \; in \; [MPa] \quad (53)$$

For confined concrete, Confinement only affected the slope of the post-peak branch and is given by

$$f_{ci} = f_c'\,[1 - z(\varepsilon_{ci} - \varepsilon_{co})] \quad (54)$$

$$z = \frac{0.5}{\varepsilon_{50h} + \varepsilon_{50u} - \varepsilon_{co}} \quad (55)$$

$$\varepsilon_{50h} = \varepsilon_{50c} - \varepsilon_{50u} = \frac{3}{4}p''\sqrt{\frac{b''}{s}}$$
$$\varepsilon_{50u} = \frac{3 + 0.29f_c'}{145f_c' - 1000} \quad , f_c' \; in \; [MPa] \quad (56)$$

where ε_{50c} and ε_{50u} are the strains corresponding to the stress equal to 50% of the maximum concrete strength for confined and unconfined concrete, respectively. $\frac{b''}{s}$ is the ratio between the width of the concrete core and the center to center spacing of hoops, p'' is the volumetric ratio of confining hoops to volume of concrete core measured to the outside of the perimeter hoops and is expressed as:

$$p'' = \frac{2(b'' + d'')As''}{b''d''s} \quad (57)$$

where b'' and d'' are the width and depth of the confined core respectively, As'' is the cross-sectional area of the hoop bar and s is the center to center spacing of the hoops.

4.1.2 Tension

Early models for concrete in tension were based on a single parameter that tensile strength (cracking stress) of concrete. This simple representation is not supported by test results and when used in finite element codes is gives inconsistent results depending on mesh size. Recently, several attempts have been made to propose an idealized tensile softening model, in which a concrete exhibits a gradual decrease in stress with increasing crack opening. Some of common types of tension softening models were shown in Figure 10. In the present paper linear and the exponential softening patterns are used [12]. The exponential function for concrete response in tension after cracking involving limiting value of ultimate tensile strain based on crack facture energy.

$$f_t = \begin{cases} E_c\varepsilon & \varepsilon \le \varepsilon_{cr} \\ f_{cr}\,exp\left(-\dfrac{\varepsilon - \varepsilon_{cr}}{\varepsilon_{tu} - \varepsilon_{cr}}\right) & \varepsilon_{cr} < \varepsilon < \varepsilon_{tu} \\ 0 & \varepsilon > \varepsilon_{tu} \end{cases} \quad (58)$$

where, ε_{tu} is the ultimate tensile strain which is determined from the tensile fracture energy G_f and determined from

$$\varepsilon_{tu} = \frac{G_f}{h f_{cr}} + 0.5\varepsilon_{cr} \quad (59)$$

where h is the crack band width and related to the area of the finite element, A, by the following relation

$$h = \alpha\sqrt{A} \quad (60)$$

where $\alpha = \sqrt{2}$ is factor with a suggested value [12].

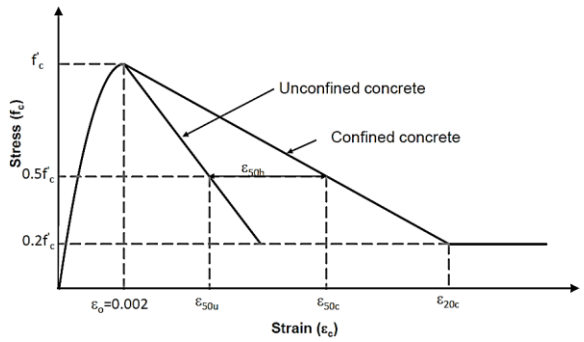

Figure 9: Stress-strain model for confined and unconfined concrete [10].

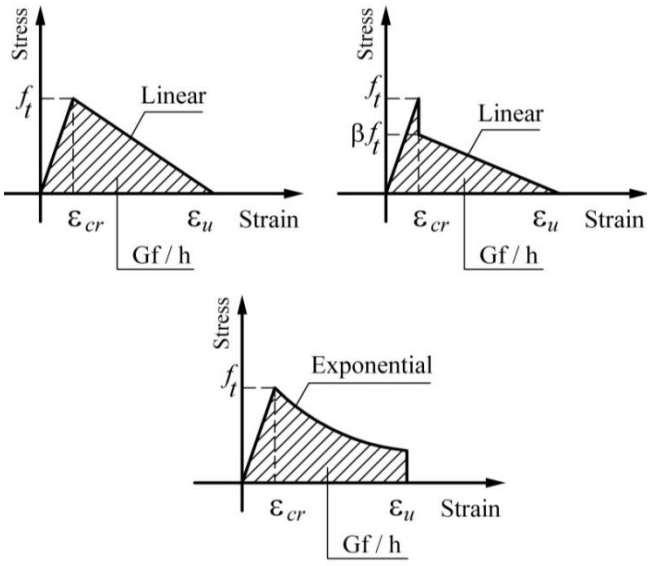

Figure 10: Common types of tension stiffening models [12].

4.2 Reinforcing Steel Constitutive Laws

The first idealization neglects the strength increase due to strain hardening and the reinforcing steel is modeled as a linear, perfectly plastic material, as shown in (Figure 11-a). More accurate idealizations which account for the strain hardening effect are required, as shown in Figure 11-b. The parameters of these models are the stress and strain at the onset of yielding (f_y ,ε_y), the strain at the onset of strain hardening and the stress and strain at ultimate (f_{max}, ε_u). These parameters can be derived from experimentally obtained stress-strain relations.

$$f_s = \begin{Bmatrix} E_S\,\varepsilon \\ f_y + bE_S(\varepsilon - \varepsilon_y) \\ 0 \end{Bmatrix} \begin{matrix} \varepsilon \le \varepsilon_y \\ \varepsilon_y < \varepsilon \le \varepsilon_u \\ \varepsilon > \varepsilon_u \end{matrix} \quad (61)$$

where E_S is the initial tangent modulus for steel material, f_y is the yield strength for reinforcement steel, b is the hardening tangent modulus ratio, and ε_u is the ultimate strain of reinforcement steel.

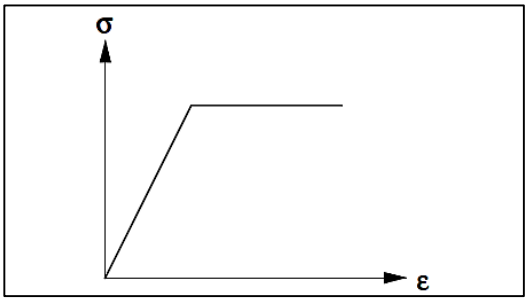

(a) elastic-perfect plastic model

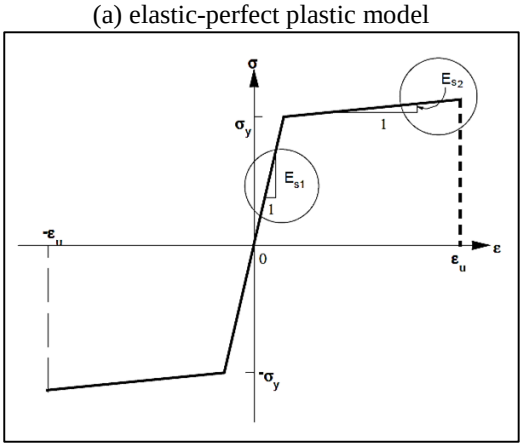

(b) elastoplastic with strain hardening ratio

Figure 11: Idealized steel stress-strain relation [2]

4.3 Concrete Hysteric Model

Different models for concrete hysteretic behavior were presented and discussed in the literature. In the present research some simplifications for the model presented by He [12] were made. A linear loading/reloading paths from tension or compression domains were assumed, Figure 12-a. The plastic compressive and tensile strains are calculated from:

$$\varepsilon_c^{pl} = \varepsilon_c^{min} - \frac{20}{7}\left[1 - exp\left(-0.35\frac{\varepsilon_c^{min}}{\varepsilon_c^{o}}\right)\right]\varepsilon_c^{o} \quad (62)$$

$$\varepsilon_t^{pl} = \begin{cases} 0 & \varepsilon_t \le \varepsilon_t^{cr} \\ 0.9\varepsilon_t^{\max} - 0.8\varepsilon_t^{cr} & \varepsilon_t < \varepsilon_t^{cr} \end{cases} \quad (63)$$

where ε_c^{min} and ε_c^{o} are the maximum experienced compressive strain and strain corresponding to peak stress on the compression envelope curve. $\varepsilon_t^{\max}$ and ε_t^{cr} are the maximum experienced tensile strain and

cracking strain of concrete. Under reversed cyclic loading, concrete may repeatedly experience crack closing and reopening. Hence, we need to define a path for the process. The stress required to cause crack close can be expressed as follows:

$$\sigma_{crack}^{close} = -f_t\left(0.05 + \frac{0.03{\varepsilon_t}^{max}}{{\varepsilon_t}^{cr}}\right) \quad (64)$$

The path of the crack closing is illustrated by a straight line that connects points **TE** and **TU**, as shown in Figure 12-b.

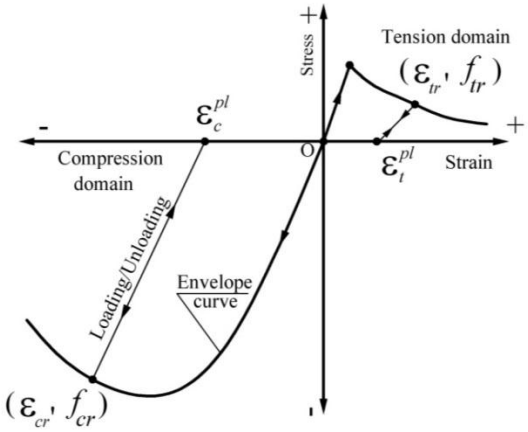

(a) Linear unloading/reloading paths

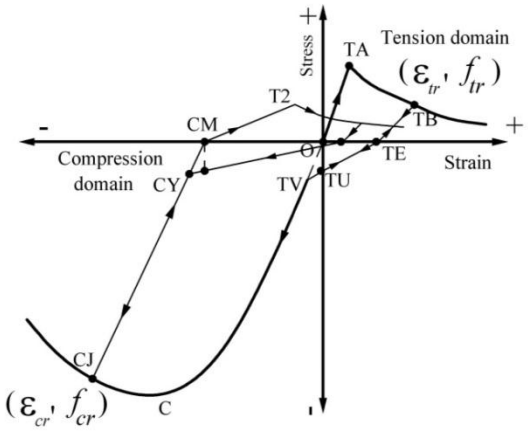

(b) transition from compression to tension

Figure 12: Proposed modification for concrete hysteretic behavior on He model [12].

4.4 Reinforcing Steel Hysteric Model

Previous research shows that the Menegotto-Pinto equation represents well the unloading and reloading response of reinforcing steel subjected to cyclic loading. The model as presented in Menegotto [13] is used in the present work as follows:

$$f^* = b.\varepsilon^* + \frac{(1-b).\varepsilon^*}{(1+\varepsilon^{*R})^{1/R}} \quad (65)$$

$$\varepsilon^* = \frac{\varepsilon - \varepsilon_r}{\varepsilon_o - \varepsilon_r} \quad (66)$$

$$f^* = \frac{f - f_r}{f_o - f_r} \quad (67)$$

Eq. (65) represents a curved transition from a straight line asymptote with slope E_0 to another asymptote with slope E_1 (lines (a) and (b), respectively, in Figure 13-a), and ε_o are the stress and strain at the point where the two asymptotes of the branch under consideration meet (point B in Figure 13-a); similarly, σ_r and ε_r are the stress and strain at the point where the last strain reversal with stress of equal sign took place (point A in Figure 13-a); b is the strain hardening ratio, that is the ratio between slope E_1 and E_0 and R is a parameter that influences the shape of the transition curve and allows a good representation of the Bauschinger effect.

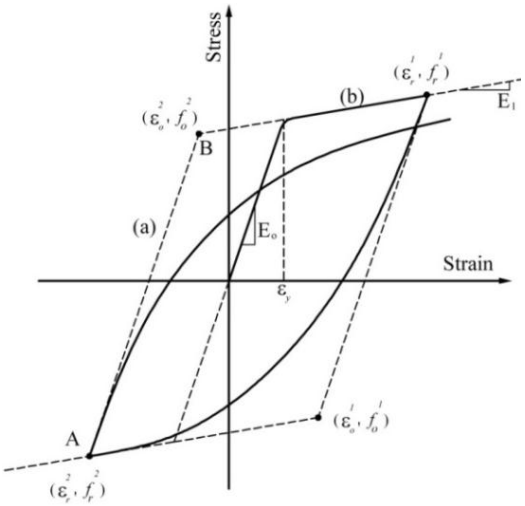

(a) transition from linear-elastic to plastic after yield

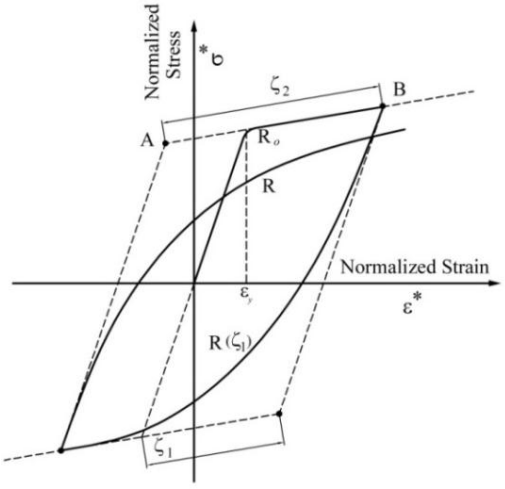

(b) definition of parameter "R"

Figure 13: Menegotto-Pinto steel model [13].

As indicated in Figure 13-a, (ε_o , σ_o) and (ε_r , σ_r) are updated after each strain reversal. R is considered dependent on the strain difference between the current asymptote intersection point (point A in Figure 13-b)

and the previous load reversal point with maximum or minimum strain depending on whether the corresponding steel stress is positive or negative (point B in Figure 13-b). The expression for R takes the form

$$R(\xi) = R_o - \frac{a_1 \xi}{a_2 + \xi} \qquad [13] \tag{68}$$

where ξ is updated following a strain reversal. R_o is the value of the parameter R during first loading and a_1, a_2 are experimentally determined parameters to be defined together with R_o. The definition of ξ remains valid in case that reloading occurs after partial unloading and calculated from

$$\xi = \begin{cases} \left| \dfrac{\varepsilon_{st}^{max} - \varepsilon_0}{\varepsilon_{sy}} \right| & d\varepsilon > 0 \\ \left| \dfrac{\varepsilon_{st}^{min} - \varepsilon_0}{\varepsilon_{sy}} \right| & d\varepsilon < 0 \end{cases} \tag{69}$$

In the present research the parameter values are taken as follows: $R_0 = 20$, $a_1 = 18.5$, $a_2 = 0.15$.

5. Model Verification

For the sake of verification, the predicated results using the developed element were compared against those theoretical and experimental published results available in the literature.

5.1 Monotonic Moment Curvature Response

The modified compression field theory (MCFT) was used to calculate the behavior of reinforced concrete sections under monotonic and uniaxial bending, normal and shear forces and it was implemented in a computer program called Response-2000 [14]. The first comparison is made on a beam has a breadth of 300 mm and a height 0f 300 mm, it is reinforced by 12 bars with diameter 12mm, distributed evenly al around the section Figure 14-a. The moment-curvature relationship comparison between present study and *Response-2000* is shown in Figure 14-b. A very good agreement is realized.

5.2 Cyclic Moment Curvature Response

The cantilever beam tested by Kent and subjected to cyclic end point load (displacement) is studied [15]. The geometry of the beam and cross section are found Kent [15]. The material properties for the beam are shown in Figure 15-a. In this example the tensile strength of concrete and tension stiffening are considered. The beam was modeled with a single element using the modified flexibility formulation developed in this study. A Simpson's integration scheme was used with 8 integration points along the element. In the transverse direction, integration was calculated by 60 layers over the section depth. The moment-curvature diagram of the fixed end section obtained from the tangent stiffness formulations is shown in Figure 15-b. Figure 15-b shows a good correlation against the experimental test results [15] and the theoretical results obtained by Valipour [5]. It addition, the tensile strength of concrete and the tension stiffening model has a limited effect on the shape of cyclic moment-curvature relation after the first cycle. Moreover, the shape of the moment-curvature is affected considerably by the hysteric properties of reinforcing steel.

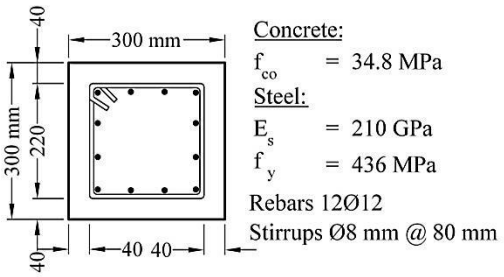

(a)

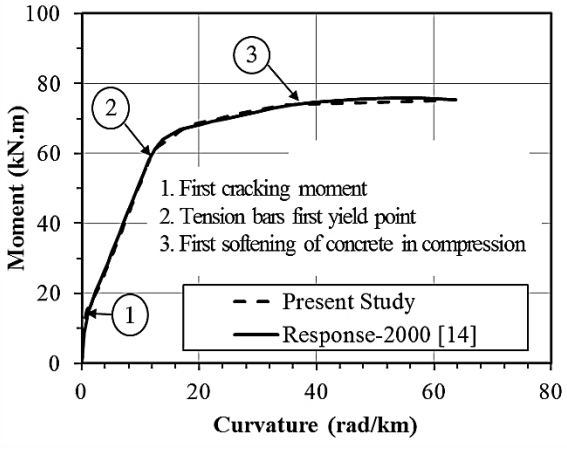

(b)

Figure 14: (a) Beam x-section details and material properties [14], (b) moment-curvature relationship comparison between present study and Response-2000

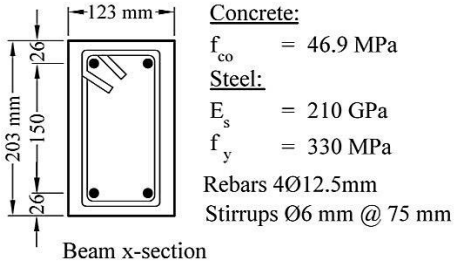

(a)

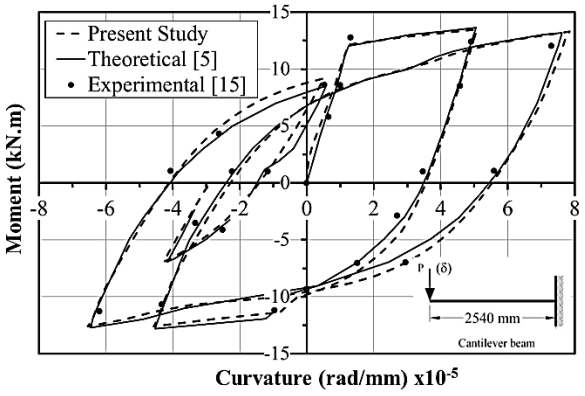

(b)

Figure 15: (a) Cantilever beam x-section details and material properties [15], (b) Moment curvature relationship for section at the fixed end.

5.3 Cyclically Loaded Beam to Column Joint

The beam column subassemblage designed and tested by Soleimani [16] was a half scale model of a cruciform shaped portion from the third story of a twenty story, four bay ductile moment-resisting frame. In the original report [16], it is designated as specimen BC3. The design was based on the strong column-weak girder design philosophy and the joint was designed so as to minimize the effects of shear transfer. The specimen geometry and reinforcement layout are shown in Figure 16. The subassemblage was subjected to constant gravity load and cyclic lateral displacement of gradually increasing magnitude. The scheme of load application is shown in Figure 16. The concentrated rotations which take place at the beam column interface due to slippage of the reinforcing bars anchored in the joint were measured with eight precision linear potentiometers, more details for method of measurement for fixed end rotations could be found in Soleimani [16].

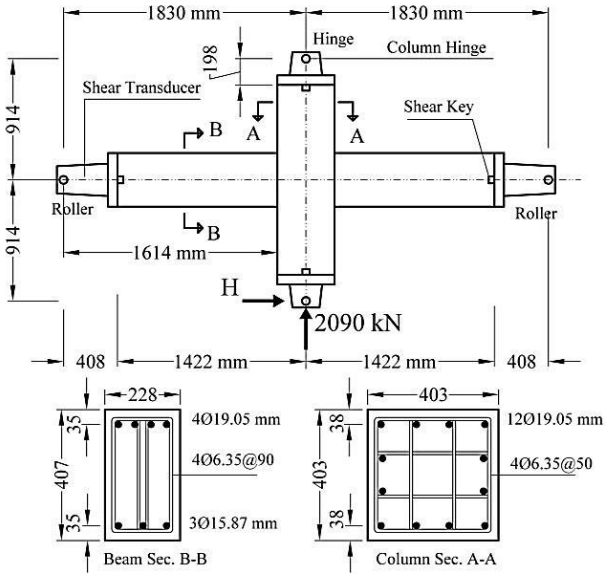

Figure 16: Beam column joint test specimen [16]

The model used in the current analytical investigation consists of two beam elements and two column elements. The beam elements are each made up of flexibility- based beam column, rotational spring, and rigid zones (end offset), Figure 17a. The material properties for both concrete and reinforcement used in the current joint are summarized in Table 1. The properties of the rotational springs are determined using the joint model by Filippou [2], Figure 17b. Using test measurements at beam column interface by soleimani [16], the bilinear moment-rotation relation at the beam column joint interface of specimen BC3 which is evaluated by Filippou [2] is summarized in Table 2.

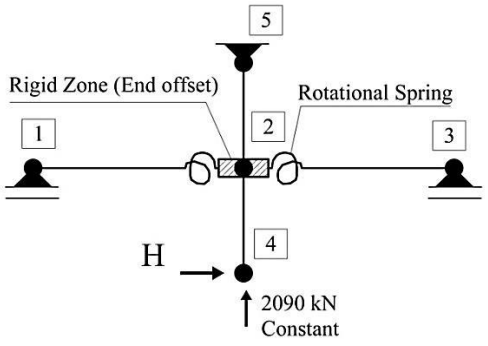

(a)

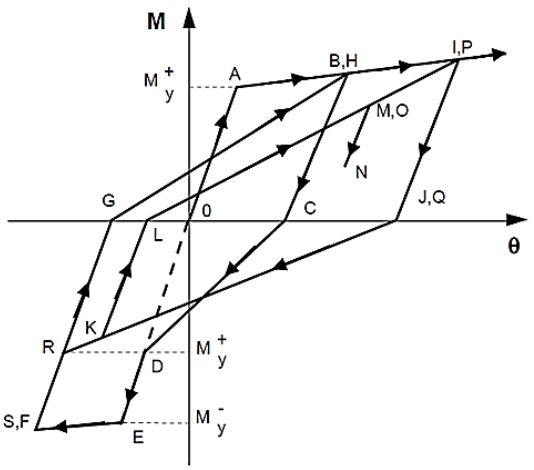

(b)

Figure 17: (a) Finite element modeling of joint test specimen, (b) Moment rotation model for rotation end spring [2].

While the joint specimen is tested experimentally by applying horizontal cyclic displacement, the finite element model shown in Figure 17 is analyzed by applying cyclic load history, Figure 18.

Table 1: Material properties and stress strain curves for joint specimen [16].

Material	**Material Modeling**
Concrete	Compression: Kent and Park [10] model, E_c = 28.5 GPa, $f_{c'}$ =f_{co}= 36 MPa Tension: Linear softening ε_{tu} = 0.001, f_t = 3.0 MPa Hysteretic Model: Simplified He [12] (subsection 4.3)
Reinforcement	Bilinear with 3.4% strain hardening ratio, F_y = 450 MPa, E_s = 200 GPa Hysteretic Model: Menegotto-Pinto [13] (subsection 4.4)

Table 2: Moment rotation relation at the beam column interface by Filippou [2].

Direction	**Moment rotation relation-ship.**
Positive moment (tension at beam bottom fiber, low reinforcement)	Bilinear with 5% strain hardening ratio M_y+ = 99 kN.m, initial stiffness= 46210 kN.m/rad.
Positive moment (tension at beam top fiber, high reinforcement)	Bilinear with 3.4% strain hardening ratio M_y- = 177 kN.m, initial stiffness= 82254 kN.m/rad.

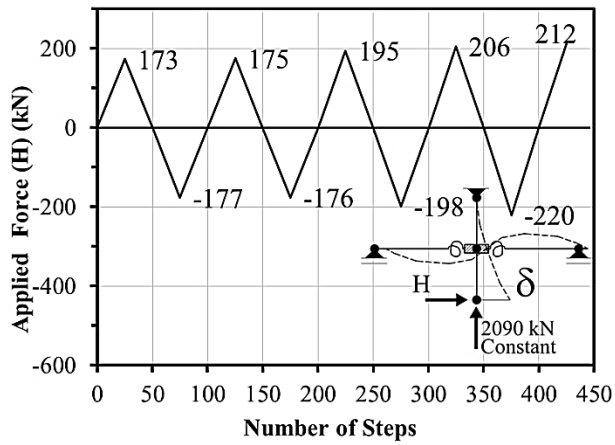

Figure 18: Analytical loading history for the investigated joint specimen.

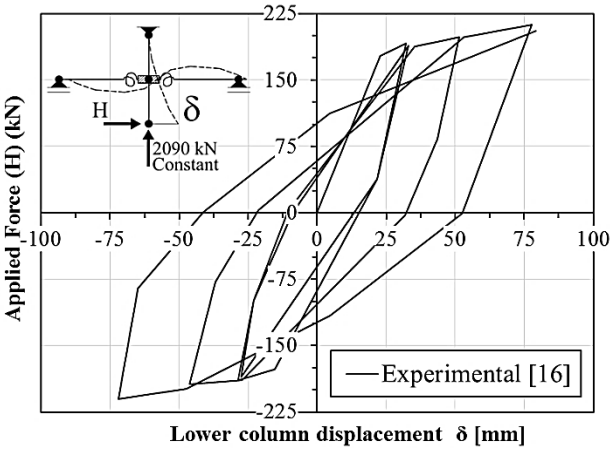

Figure 19: Experimental load-displacement relationship [16].

The analytical predictions of the frame model described in Figure 17-a subjected to the load history illustrated in Figure 18 are shown in Figures 19 and 20. Figure 20 shows the load-displacement relationship measured at the bottom of the column in Figure 16. Even though the experiment was conducted under displacement controlled conditions, the analysis was performed by specifying the magnitude of the lateral load measured at the moment of load reversal and then subdividing this load into a number of increments. The predicted results from the present study show a very good correlation with the experimental investigation.

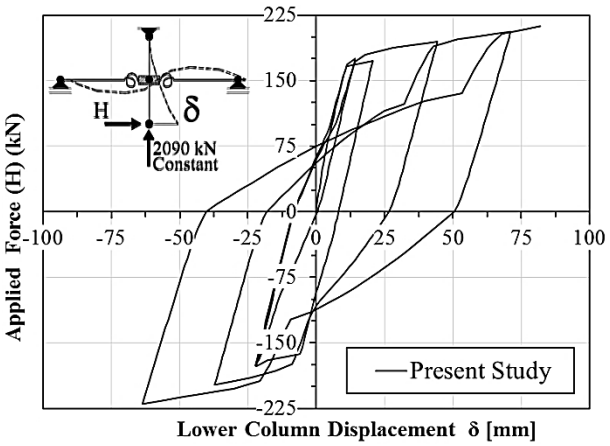

Figure 20: Predicted load-displacement relationship for the joint specimen.

5.4 Effect of Section Centroid Update

To illustrate the effect of the original formulation by Taucer [3] and the revised procedure in the present study, a 6.0 ms spanned reinforced concrete simple beam with 300x500 mm^2 cross section, Figure 21, is analyzed. The beam is provided with 5Φ18 mm as tension steel and 2Φ16 mm compression steel. The beam was nonlinearly analyzed under monotonic increasing mid-span load up to failure.

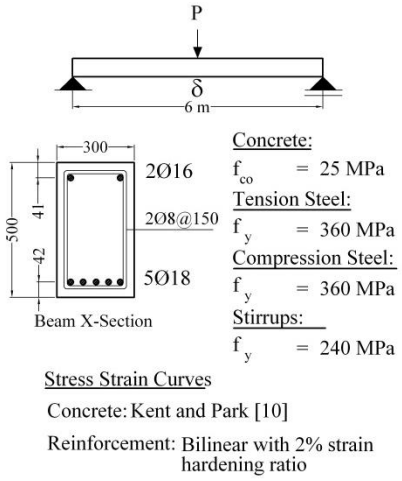

Figure 21: Reinforced concrete beam elevation, cross-section, and material properties

According to loading configurations shown in Figure 21, there will be no horizontal displacement at the roller end whereas the beam is modeled using line element. From Figure 22, the proposed formulation reduced the analysis error significantly specially after cracking and prior to failure. The analyses errors produced from formulation assumptions could be reduced much more if section center of gravity is updated continuously while performing Newton Raphson correction process. In the present work, the center of gravity updating scheme was performed only at the beginning of each loading step due to convergence issues.

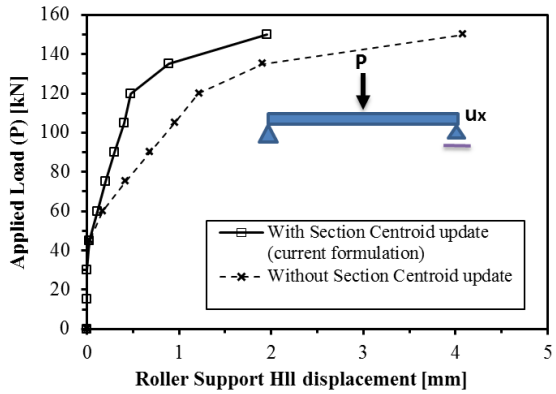

Figure 22: Horizontal displacement at the roller end using the proposed formulation.

6. Conclusions

Based on proposed formulation and analysis, the following conclusions could be drawn:

- A flexibility-based beam column element, with extended features as end springs to account for semi-rigid connections and end offsets, is presented. A revised solution procedure is proposed to minimize analysis errors from the continuously changing neutral axis location during the analysis. The element state determination, with/without end springs or end offsets, is presented. The element is implemented into a finite element computer program in order to study nonlinear static and dynamic analysis of reinforced concrete frames. The correlation analysis showed a good agreement with theoretical/experimental published studies for both monotonic and cyclic loading conditions.
- A simplified hysteretic model for concrete is proposed with crack closing and opening effects.
- Steel reinforcing bars have a significant influence on the hysteretic behavior of RC structures, such as pinching effect, Figure 15-b. Hence, the bond-slip and the buckling of steel reinforcement should be modeled in the future.

7. References

[1] Kaba, S., & Mahi, S. (1984). Refined Modeling of Reinforced Concrete Columns of Seismic Analysis. CA.: ECRC Report 84-00, Earthquake Engineering Research Inst., Berkeley.

[2] Filippou, F. C., & Issa, A. (1988). Nonlinear Analysis of Reinforced Concrete Frames under Cyclic Load Reversals. Berkeley: Report No. UCB/EERC–88/12, Earthquake Engineering Research Center, College of

Engineering, University of California.
[3] Taucer, F. F., Spacone, E., & Filippou, F. C. (1991). A Fiber Beam Column Element for Seismic Response Analysis of Reinforced Concrete Structures. Report No. UCB/EERC-91/17,Earthquake Engineering Research Center, College of Engineering, University of California, Berkeley.
[4] Monti, G., & Spacone, E. (2000). Consistent insertion of bond-slip into beam fiber elements for biaxial bending. 12th World Conference on Earthquake Engineering . Auckland.
[5] Valipour, H. R., & Foster, S. J. (2007). A Novel Flexibility-Based Beam Column Element For Nonlinear Analysis of Reinforced Concrete Frames. The University of New South Wales: UNICIV Report No. R-447,ISBN : 85841 414 7.
[6] Diotallevi, P. P., Landi, L., & Cardinetti, F. (2008). A Fibre Beam Column Element for Modeling the Flexure-Shear Interaction in the Nonlinear Analysis of RC Structures. The 14th, World Conference on Earthquake Engineering. Beijing, China.
[7] Mohr, S., Bairán, J. M., & Marí, A. R. (2010). A frame element model for the analysis of reinforced concrete structures under shear and bending. Engineering Structures, 3936-3954.
[8] El-Heweity, M., Mashaly, E.-S., & Abou-Elfath. (2011). A new beam column model for seismic analysis of RC frames – Part I: Model derivation. Alexandria Engineering Journal, 313-320.
[9] Lowes, L. N., & Altoontash, A. (2003). Modeling Reinforced-Concrete Beam Column Joints Subjected to Cyclic Loading. JOURNAL OF STRUCTURAL ENGINEERING © ASCE, 1686-1697.
[10] Kent, D., & Park, R. (1971). Flexural members with confined concrete. Journal of the Structural Division, Proc. of the American Society of Civil Engineers, 97,ST7, 1969-1990, Vols. 97,ST7, 1969-1990.
[11] Hognestad, E. (1951). A study on combined bending and axial load in reinforced concrete members. Univ. of Illinois at Urbana-Champaign, IL, 43-46: Univ. of Illinois Engineering Experiment Station.
[12] He, W., Wu, Y.-F., & Liew, K. (2008). A fracture energy based constitutive model for the analysis of reinforced concrete structures under cyclic loading. 197 - p4745–4762.
[13] Menegotto, M., & Pinto, P. E. (1973). Method of analysis for cyclically loaded R.C. plane frames including changes in geometry and non-elastic behavior of elements under combined normal force and bending. Roma, Italy: IABSE reports of the working commissions.
[14] Bentz, E. C. (2000). Sectional Analysis of Reinforced Concrete Members. PhD thesis, Department of Civil Engineering, University of Toronto, Ottawa, Canada.
[15] Kent, D. C. (1969). Inelastic behavior of reinforced concrete members with cyclic. PhD. Dissertation, University of Canterbury, Christchurch, New Zealand.
[16] Soleimani, D., Popov, E., & Bertero, V. (1979). Hyestertic Behaviour of Reinforced Concrete Beam Column Subassemblages. 76, No. 11(pp. 1179, 1195).